Rapid Communications

Tunable interlayer magnetism and band topology in van der Waals heterostructures of $MnBi_2Te_4$-family materials

Zhe Li,[1,2] Jiaheng Li,[1,2] Ke He,[1,2,3,*] Xiangang Wan,[4,5] Wenhui Duan,[1,2,3,6] and Yong Xu[1,2,7,†]

[1]*State Key Laboratory of Low-Dimensional Quantum Physics, Department of Physics, Tsinghua University, Beijing 100084, China*

[2]*Frontier Science Center for Quantum Information, Beijing 100084, China*

[3]*Beijing Institute of Quantum Information Science, Beijing 100193, China*

[4]*National Laboratory of Solid State Microstructures and School of Physics, Nanjing University, Nanjing 210093, China*

[5]*Collaborative Innovation Center of Advanced Microstructures, Nanjing 210093, China*

[6]*Institute for Advanced Study, Tsinghua University, Beijing 100084, China*

[7]*RIKEN Center for Emergent Matter Science (CEMS), Wako, Saitama 351-0198, Japan*

(Received 28 May 2020; accepted 29 July 2020; published 11 August 2020)

Manipulating interlayer magnetic coupling (IMC) of van der Waals (vdW) magnets is the key to tailoring material properties for various electronic applications and fundamental studies. Using $MnBi_2Te_4$-family materials as examples, we systematically investigate the constituent-element dependence of IMC by first-principles calculations and attribute the IMC to unusual long-range superexchange interactions mediated by the *p* orbitals across the vdW gap. Remarkably, a simple, universal rule is proposed to determine the sign of IMC (ferromagnetic or antiferromagnetic) by *d*-orbital occupation, and guidance is provided to achieve extraordinarily strong or stacking-dependent IMC by element engineering. Furthermore, several magnetic topological states are designed by heterostructuring, including ferromagnetic Weyl semimetals, high-order topological insulators, and unusual kinds of quantum anomalous Hall insulators. The findings enable us to engineer the magnetic and topological properties of $MnBi_2Te_4$-family materials as well as other vdW magnetic materials and heterostructures.

DOI: 10.1103/PhysRevB.102.081107

Over the past few years, van der Waals (vdW) layered magnets have attracted intensive attention [1–7]. Benefitting from weak interlayer interactions, these materials can be easily exfoliated into ultrathin flakes and flexibly recombined into various heterostructures with novel material properties. Many layered magnetic materials have been found, including $Cr_2Ge_2Te_6$, CrI_3, Fe_3GeTe_2, $FePS_3$, VSe_2, $MnSe_2$ [3,4,8–14], and the $MnBi_2Te_4$-family compounds [15–26], which provide new chances for developing electronics, spintronics, optoelectronics, as well as topological physics and applications [5–7,15–31]. A key ingredient to designing and engineering vdW magnetic materials and heterostructures for various purposes is to manipulate the interlayer magnetic coupling (IMC), i.e., the magnetic coupling across the vdW gap. The sign and magnitude of IMC have been found to vary significantly in different vdW magnets. Despite some preliminary research [3,8–13], a comprehensive understanding of the underlying mechanism is still lacking.

The $MnBi_2Te_4$-family compounds as vdW layered intrinsic magnetic topological materials are particularly interesting due to the rich magnetic topological phases they host, including an antiferromagnetic (AFM) topological insulator (TI) [15–26,31] and a magnetic Weyl semimetal (WSM) [15,17,18,26] in the three-dimensional (3D) bulk, as well as a quantum anomalous Hall (QAH) insulator [15–21,25,26] and axion insulator [15–20] in their 2D films. Quantized transport has been observed in $MnBi_2Te_4$ thin flakes at relatively high temperatures (>1 K) [20,21,25]. Crystallized in a rhombohedral layered structure, bulk tetradymite-type $MnBi_2Te_4$ is composed of vdW-bonded septuple layers (SLs). Each SL consists of seven atomic layers, of a triangular lattice with *ABC* stacking in a sequence of Te/Bi/Te/Mn/Te/Bi/Te. The intralayer magnetic coupling is ferromagnetic (FM) with an out-of-plane easy magnetic axis, while the IMC is AFM. Thus, the $MnBi_2Te_4$ bulk has an *A*-type AFM ground state.

$MnBi_2Te_4$-family materials provide an excellent platform to explore the IMC mechanism of vdW magnets. First, the ternary-compound family includes many candidate materials constituted by different combinations of nonmagnetic and magnetic elements [15], which enables a systematic study on the element dependence of IMC. Second, the relatively long distance between neighboring magnetic atomic layers forbids many kinds of electron hopping channels, and only medial *p* orbitals across the vdW gap are relevant to the IMC, simplifying the discussion on the underlying mechanism. In addition, since the topological properties of $MnBi_2Te_4$-family materials depend critically on the interlayer magnetism [15–17,20,25,26], knowledge of the IMC mechanism can be directly used to engineer magnetic topological quantum states and effects [27–31].

In this Rapid Communication we systematically study the constituent-element dependence of the IMC of

*kehe@tsinghua.edu.cn

†yongxu@mail.tsinghua.edu.cn

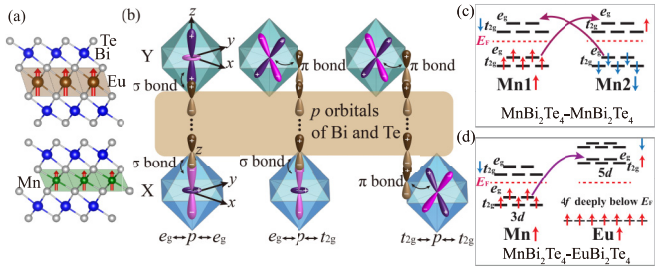

FIG. 1. Superexchange coupling in $X\mathrm{Bi_2Te_4}$-$Y\mathrm{Bi_2Te_4}$ bilayers. (a) Crystal structures (side view) of a $\mathrm{MnBi_2Te_4}$-$\mathrm{EuBi_2Te_4}$ bilayer. The red arrows indicate the spin orientations. (b) Schematic drawings of three hopping channels related to the superexchange interlayer magnetic coupling: e_g-p-e_g (left), e_g-p-t_{2g} (middle), and t_{2g}-p-t_{2g} (right). X and Y denote magnetic atoms of $X\mathrm{Bi_2Te_4}$-$Y\mathrm{Bi_2Te_4}$. (c), (d) Schematic drawings of the energy levels of magnetic atoms and the dominant hopping channels for (c) $\mathrm{MnBi_2Te_4}$-$\mathrm{MnBi_2Te_4}$ and (d) $\mathrm{MnBi_2Te_4}$-$\mathrm{EuBi_2Te_4}$.

$\mathrm{MnBi_2Te_4}$-family materials and heterostructures by first-principles calculations (see Methods in the Supplemental Material [32]). Our results reveal that the IMC is dominated by unusual long-range superexchange interactions mediated by the p orbitals of nonmagnetic atoms across the vdW gap. The sign of IMC is dictated by the d-orbital occupation, and the magnitude of IMC is significantly determined by the delocalization degree of medial p orbitals and the strength of p-d orbital hybridization. Furthermore, various magnetic topological states can be realized by constructing heterostructures of $\mathrm{MnBi_2Te_4}$-family materials in the absence of an external magnetic field, which is superior to previous ones [15,17]. These findings provide us useful guidelines to understand, design, and engineer the magnetic and topological properties not only for this material family but also for insulating vdW magnets in general.

According to the superexchange theory [39,40], the exchange coupling between two magnetic atoms emerges when an indirect electron hopping between d orbitals of magnetic elements is mediated by the connecting p orbitals. In the $\mathrm{MnBi_2Te_4}$-family compounds, each magnetic atom is bonded with six chalcogen atoms in a slightly distorted octahedral geometry, where the d orbitals are roughly split to the triply degenerate t_{2g} states and the doubly degenerate e_g states. The medial d orbitals across the vdW gap link the d orbitals of neighboring SLs, which are relevant to the IMC. Generally, there exist three kinds of hopping channels in the system, including e_g-p-e_g, e_g-p-t_{2g}, and t_{2g}-p-t_{2g}, as illustrated in Fig. 1(b). Here, σ bonds are formed between e_g and p orbitals, whose strength is much stronger than that of π bonds formed between t_{2g} and p orbitals. Therefore, the e_g-p-e_g hopping channels, if they exist, would play a dominant role in determining the IMC.

We first analyze the IMC of $\mathrm{MnBi_2Te_4}$. The five $3d$ electrons of Mn^{2+} ions fully occupy the spin-up channels, leaving the spin-down channels empty. Since each SL is an FM insulator, as found previously [15,16,41], the key issue is to compare the energies of two configurations with magnetic moments of neighboring SLs aligned parallel and antiparallel with each other (hereafter called FM and AFM configurations for simplicity). As illustrated in Fig. 1(c), the virtual hopping between d orbitals of two neighboring SLs is allowed in the AFM configuration, but prohibited by the Pauli exclusion principle in the FM configuration. Therefore, the AFM configuration is energetically more favorable, leading to an AFM IMC and an A-type AFM ground state in $\mathrm{MnBi_2Te_4}$, consistent with previous theoretical and experimental results [15–20,22–24]. Similar analyses on other $\mathrm{MnBi_2Te_4}$-family compounds, including $X(\mathrm{V})_2(\mathrm{VI})_4$ [X = Mn, V, Ni, or Eu; (V) = Bi or Sb; (VI) = Te, Se, or S], indicate that their IMC is always AFM, independent of constituent elements, as confirmed by our first-principles calculations. This seems to be a disadvantage for research and applications, since sometimes FM IMC is desired, for instance, for realizing FM topological states (e.g., WSMs, high-Chern-number QAH insulators) or effects (e.g., anomalous Hall effects, anomalous transverse thermoelectric effects) without applying a magnetic field.

TABLE I. The magnetic ground states and the interlayer exchange energies (E_{ex}) defined as the energy difference per formula unit between the A-type AFM and FM configurations of $X\mathrm{Bi_2Te_4}$-$Y\mathrm{Bi_2Te_4}$ bilayers, where $X(Y)$ = Ni, Mn, V, Eu.

		X			
	E_{ex}/(meV)	Ni($3d^8$)	Mn($3d^5$)	V($3d^3$)	Eu($4f^7+5d^0$)
Y	Ni($3d^8$)	AFM	AFM	**FM**	**FM**
		−16.5	−5.4	**+2.5**	**+1.1**
	Mn($3d^5$)	AFM	AFM	**FM**	**FM**
		−5.4	−1.3	**+1.1**	**+0.5**
	V($3d^3$)	**FM**	**FM**	AFM	AFM
		+2.5	**+1.2**	−0.5	−0.2
	Eu($4f^7+5d^0$)	**FM**	**FM**	AFM	AFM
		+1.1	**+0.5**	−0.2	−0.1

In contrast to pure compounds, the IMC of vdW heterostructures of $\mathrm{MnBi_2Te_4}$-family materials has been rarely explored as far as we know, which could offer different degrees of freedom to tuning magnetic and topological properties. Take the $\mathrm{MnBi_2Te_4}$-$\mathrm{EuBi_2Te_4}$ combination as an example [Fig. 1(a)]. In $\mathrm{EuBi_2Te_4}$, the $4f$ orbitals of Eu are far away from the Fermi level (E_{F}), leaving the $5d$ orbitals close to E_{F}. These $5d$ orbitals are empty and polarized by magnetic moments of the $4f$ electrons, giving spin-up states lower than spin-down states [42]. Although e_g-p-e_g hopping is allowed in both FM and AFM configurations, the virtual hopping between spin-up e_g orbitals of Mn and Eu atoms is energetically more favorable in the FM configuration, benefitting from the on-site Coulomb exchange of Eu [Fig. 1(d)]. Other hopping channels are allowed as well, whose contributions to IMC are relatively smaller and of the same sign (see details in the Supplemental Material [32]). Therefore, the magnetic ground state is FM, in agreement with our first-principles result with the energy difference between the interlayer AFM and FM configurations per formula unit (E_{ex}) +0.5 meV.

We considered all the possible combinations of $X\mathrm{Bi_2Te_4}$-$Y\mathrm{Bi_2Te_4}$ bilayers (X, Y = Mn, V, Ni, Eu) and summarized their calculated magnetic energies (E_{ex}) in Table I. Remarkably, the sign of IMC is closely

related to the d-orbital occupations of magnetic elements X and Y. The magnetic elements are classified into two groups according to the d-orbital occupation: A (less than half filled) and B (half filled or more). The IMC of $X\mathrm{Bi_2Te_4}$-$Y\mathrm{Bi_2Te_4}$ is AFM between A-A or B-B, whereas it is FM between A-B, giving a simple rule to determine the sign of IMC. The result is consistent with the analysis based on the superexchange theory (see Supplemental Tables S5 and S6 and Fig. S2). As the qualitative analysis depends insensitively on material details, such as the type of nonmagnetic elements or atomic structures, the above rule is expected to be generally applicable to insulating vdW magnets, as verified by our further test calculations on $X\mathrm{Bi_2Te_4}$-$\mathrm{CrI_3}$ and $X\mathrm{Bi_2Te_4}$-$\mathrm{Cr_2Ge_2Te_6}$ heterostructures (Table S7). Note that systems with weak IMC involve competing hopping channels favoring opposite signs of IMC, which are significantly stacking dependent (see details in the Supplemental Material [32]).

Noticeably, the superexchange coupling in magnetic oxides is supposed to be rather short ranged [39,40]. Typically, only the cation-anion-cation coupling is considered. Distinctly, the calculated IMC strength between $\mathrm{MnBi_2Te_4}$-family materials is not negligible though the magnetic atoms from neighboring SLs are spaced by six nonmagnetic atoms together with a vdW gap. Unexpectedly, $|E_{\mathrm{ex}}|$ between two $\mathrm{NiBi_2Te_4}$ SLs is as high as 16.5 meV. According to the superexchange theory [39,40], the strength of IMC depends critically on the orbital overlap and transfer integrals between cations and anions. In general, the more covalent (ionic) the bonds, the stronger (weaker) is the superexchange interaction. The covalency of bonds is closely related to the electronegativity difference $\Delta\chi$ between anions and cations. For magnetic oxides, the electronegativity χ (by the Pauling scale) [43,44] of oxygen is 3.44 and that of a metal element is usually below 2.00. $\Delta\chi$ is so large that the medial p electrons are rather localized around oxygen. Thus, the transfer integrals would become negligibly small if a pair of cations are separated by more than one anion. In contrast, $\Delta\chi$ of $\mathrm{MnBi_2Te_4}$-family materials is much smaller, which leads to much more delocalized p electrons, facilitating unusual long-range superexchange interactions. As evidence, the relationship between $|E_{\mathrm{ex}}|$ and $\Delta\chi$ of constituent elements (V) and (VI) is plotted for $\mathrm{Ni(V)_2(VI)_4}$ compounds [(V) = Bi, Sb, and (VI) = Te, Se, S] in Fig. 2(b), which clearly shows an inverse correlation. Further analysis indicates that the magnitude of IMC is determined by the delocalization degree of medial p orbitals and the strength of p-d orbital hybridization [Figs. 2(c) and 2(d)], which can be effectively tuned by varying the nonmagnetic elements of $\mathrm{MnBi_2Te_4}$-family materials (see details in the Supplemental Material [32]).

The understanding of the IMC mechanism of $\mathrm{MnBi_2Te_4}$-family materials enables us to design and engineer topological states by controlling the IMC. For example, $\mathrm{MnBi_2Te_4}$ with an AFM TI ground state becomes a magnetic WSM when FM-z magnetic orientation is induced by a strong out-of-plane magnetic field [15,17,18]. The obtained magnetic WSM possesses only a single pair of Weyl points, and is very useful for realizing high-Chern-number QAH phases in their thin films [25,45–49]. The FM IMC between $\mathrm{MnBi_2Te_4}$ and $\mathrm{EuBi_2Te_4}$ heterostructures suggests that one

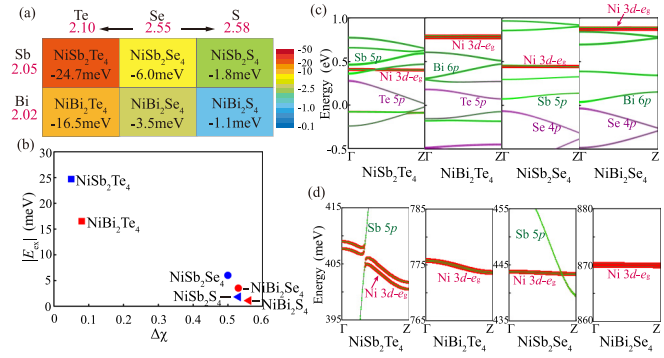

FIG. 2. Dependence of IMC of $\mathrm{Ni(V)_2(VI)_4}$ on nonmagnetic elements (V) = Bi, Sb and (VI) = Te, Se, S. (a) The IMC (E_{ex}) of $\mathrm{Ni(V)_2(VI)_4}$ bilayers. Red numbers denote the electronegativities (χ) of elements. (b) Dependence of $|E_{\mathrm{ex}}|$ on the electronegativity difference ($\Delta\chi$) between the anions (VI) and nonmagnetic cations (V) for $\mathrm{Ni(V)_2(VI)_4}$ bilayers. (c) Band dispersions of bulk $\mathrm{Ni(V)_2(VI)_4}$ along the Γ-Z direction together with orbital projection. Contributions of Ni 3d, (V) p, and (VI) p orbitals are colored red, green, and purple, respectively. (d) Zoom-in bands contributed by Ni 3d orbitals.

may obtain an intrinsic ferromagnetic WSM (with no need for applying external magnetic fields) in $\mathrm{MnBi_2Te_4}$-$\mathrm{EuBi_2Te_4}$ heterostructures.

Figure 3(a) displays the calculated bulk band structure of the $\mathrm{MnBi_2Te_4}$-$\mathrm{EuBi_2Te_4}$ superlattice that has an FM ground state with a magnetic easy axis along the out-of-plane

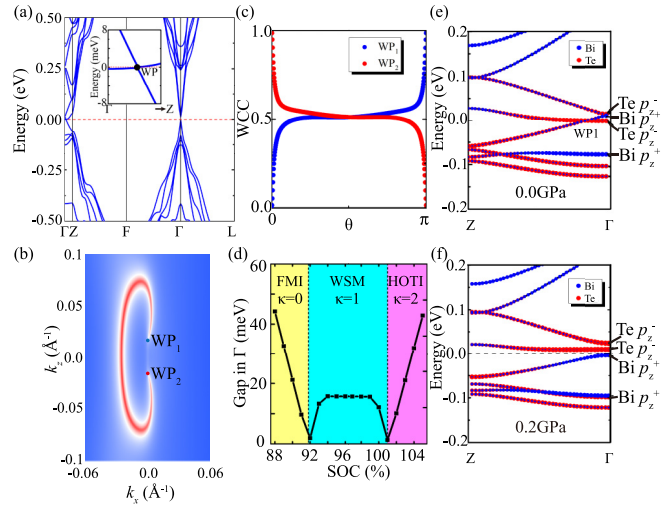

FIG. 3. Band structures and topological features of the $\mathrm{MnBi_2Te_4}$-$\mathrm{EuBi_2Te_4}$ superlattice computed by the modified Becke-Johnson functional. (a) Band structure of $\mathrm{MnBi_2Te_4}$-$\mathrm{EuBi_2Te_4}$ bulk. The inset magnifies bands near the Fermi level. (b) Surface states on the (110) plane, showing the two Weyl points ($\mathrm{WP_1}$ and $\mathrm{WP_2}$) connected by a Fermi arc. (c) The motions of the sum of Wannier charge centers (WCCs) on a sphere surrounding each Weyl point in the momentum space. (d) Direct band gap at Γ as a function of the strength of spin-orbit coupling (SOC). (e), (f) Band dispersions along the Γ-Z direction together with orbital projection under hydrostatic pressure of (e) zero and (f) 0.2 GPa. "±"denotes the even/odd parity of Bloch states.

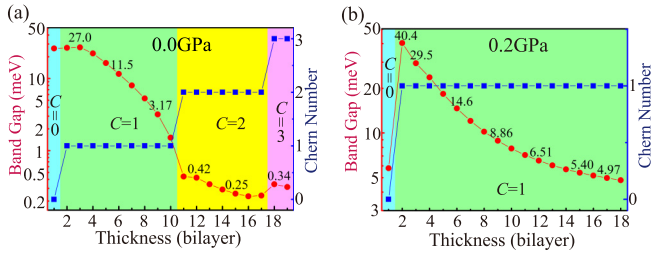

FIG. 4. Thickness-dependent topological properties of thin films of the $MnBi_2Te_4$-$EuBi_2Te_4$ superlattice. Direct band gap at Γ (red) and topological Chern number (blue) for the systems under a hydrostatic pressure of (a) zero and (b) 0.2 GPa.

direction (Table S4 and Fig. S1). A type-I Weyl point (WP) located exactly at E_F is formed by band crossing along the Γ-Z direction near the Γ point, without the coexistence of an electron and hole pocket. By checking the motions of the sum of Wannier charge centers, the two WPs show opposite chiralities, as theoretically expected [Fig. 3(c)]. The calculated surface states on the (100) plane in Fig. 3(b) clearly show a Fermi arc connecting two WPs. In contrast, other WSMs either have multiple pairs of WPs (e.g., TaAs-family materials [50–54]) or belong to type-II WSMs including both the Fermi surface and Fermi points at E_F [15,17,55].

The evolution of band gaps at Γ as a function of the artificial SOC strength in Fig. 3(d) clearly shows that there exist two band gap closures at 92% and 102%, indicating the occurrence of topological phase transitions. The gap closing points divide the phase diagram into three colors of regions, including a trivial FM insulator phase, a WSM phase, and a FM insulator phase with band inversion. The last one is a special phase, named "FMTI," which is topologically equivalent to Cr- or V-doped $(Bi, Sb)_2Te_3$ TIs [56,57].

Since the inversion symmetry exists in the $MnBi_2Te_4$-$EuBi_2Te_4$ superlattice, a $\mathbb{Z}_4$ symmetry indicator κ can be defined by the parity criterion [58] $\kappa = \sum_{\kappa_i} \frac{n_+ - n_-}{2}$, where $n_\pm$ denotes $\pm$ parity band occupations and the summation is over all inversion-symmetric crystal momenta. $\kappa = 0, 1, 2$ correspond to the FM trivial insulator, WSM, and FMTI phases, respectively. The latter corresponds to a high-order TI (HOTI) phase with intriguing chiral boundary modes, which has been theoretically proposed but lacks suitable material candidates [59]. A topological phase diagram as a function of external pressure is presented in Supplemental Fig. S5. This material is predicted to be a WSM and becomes a HOTI under small pressures (see below) by the modified Becke-Johnson functional, whereas it is predicted to be a native HOTI by the Perdew-Burke-Ernzerhof functional plus Hubbard U (PBE+U) method (Fig. S4). Despite the discrepancy, both results suggest that the $MnBi_2Te_4$-$EuBi_2Te_4$ superlattice is a promising candidate to realize the exotic HOTI phase.

Two-dimensional thin films of a magnetic WSM can show the QAH effect with the Chern number (C) increasing with the film thickness [25,48,49]. Figure 4(a) shows the evolution of the Chern number and band gap of $MnBi_2Te_4$-$EuBi_2Te_4$ thin films with varying film thicknesses. The film emerges as a normal insulator with $C = 0$ in one bilayer, and the intrinsic QAH state with $C = 1$ from two to ten bilayers with a maximum band gap (~27.0 meV) obtained in the three-bilayer film. The intrinsic QAH state can also obtained in odd number layers (i.e., half bilayer) of $MnBi_2Te_4$-$EuBi_2Te_4$ heterostructures (Fig. S7). In a FM WSM film, the increment of the Chern number (ΔC) with film thickness in the thick limit is determined by the separation of WPs in the momentum space [25], which is about 1/7 of the width of the Brillouin zone along the Γ-Z direction, suggesting that $\Delta C = 1$ for every seven bilayers. This is consistent with the calculation result that C changes from two at 11 bilayers to three at 18 bilayers [Fig. 4(a)]. Topological edge states of a three-bilayer film and a 12-bilayer film are displayed in Fig. S6, which confirms the existence of QAH states with increasing Chern numbers.

In this material system, a moderate hydrostatic pressure can lead to a band inversion at the Γ point, resulting in a topological phase transition [48]. Under ambient pressure, there is only one band inversion between Bi p_z and Te p_z bands, which leads to a WSM phase characterized by $\kappa = 1$ [Fig. 3(e)]. An additional band inversion exists under 0.2 GPa, opening an insulating band gap [Fig. 3(f)]. The HOTI phase characterized by $\kappa = 2$ thus emerges, which would transform into the typical TI phase when the time reversal symmetry is recovered in the paramagnetic state above the Curie temperature [48]. For the FM phase, thin films thicker than two bilayers are all QAH insulators with $C = 1$, as confirmed by edge-state calculations (Fig. S6).

Different from normal 2D QAH insulators, the very thick films of HOTI are expected to show "pseudo-3D" QAH insulator states, which have gapless chiral edge states distributed not only at the edges of the top or bottom surfaces but also at the hinges along the out-of-plane direction, as required by the nature of HOTI [59]. Therefore, the system is able to show nonzero quantized anomalous Hall conductance in both in-plane and out-of-plane transport measurements, which can serve as smoking-gun proof of HOTI in experiments. Moreover, when aligning the magnetism from out of plane to in plane by a magnetic field, an alternative HOTI phase could be generated, which can also give pseudo-3D QAH insulator states. Differently, the real-space distribution of chiral edge modes is changed by the magnetic field, and so is the quantized anomalous Hall conductance, enabling the design of a "topological magnetic switch" [59].

In conclusion, we systematically studied the mechanism, sign, and magnitude of IMC of the $MnBi_2Te_4$-family compounds and heterostructures, and provided a few guiding principles to tune interlayer magnetism as summarized in the Supplemental Material [32]. Moreover, we proposed vdW heterostructures with FM IMC and exotic magnetic topological states, including type-I FM WSM, HOTI, as well as high-Chern-number and pseudo-3D QAH insulators. The understanding of the IMC mechanism implicates the principles of manipulating the interlayer magnetic configurations of insulating vdW magnets, which is valuable in exploring different magnetic topological phases and effects in them.

Note added. Recently, we became aware of a related work that theoretically studied other kinds of vdW materials and

found a similar rule to determine the sign of IMC by *d*-orbital occupation of vdW magnets [60].

We thank Rui-Xing Zhang for helpful discussions. This work was supported by the National Natural Science Foundation of China (51788104, 51661135024, 11874035, 11674188), the National Key Research and Development Program of China (2017YFA0303303, 2016YFA0301001, 2018YFA0307100, 2018YFA0305603), Tsinghua University Initiative Scientific Research Program, and the Beijing Advanced Innovation Center for Future Chip (ICFC).

Z.L. and J.L. contributed equally to this work.

[1] A. K. Geim and I. V. Grigorieva, Nature (London) **499**, 419 (2013).
[2] K. S. Novoselov, A. Mishchenko, and A. Carvalho, Science **353**, aac9439 (2016).
[3] B. Huang, G. Clark, E. Navarro-Moratalla, D. R. Klein, R. Cheng, K. L. Seyler, D. Zhong, E. Schmidgall, M. A. McGuire, D. H. Cobden *et al.*, Nature (London) **546**, 270 (2017).
[4] K. S. Burch, D. Mandrus, and J.-G. Park, Nature (London) **563**, 47 (2018).
[5] J. Zak, E. R. Moog, C. Liu, and S. D. Bader, Magn. Magn. Mater. **89**, 107 (1990).
[6] D. Zhong, K. L. Seyler, X. Linpeng, R. Cheng, N. Sivadas, B. Huang, E. Schmidgall, T. Taniguchi, K. Watanabe, M. A. McGuire *et al.*, Sci. Adv. **3**, e1603113 (2017).
[7] M. Buscema, J. O. Island, D. J. Groenendijk, S. I. Blanter, G. A. Steele, H. S. J. van der Zant, and A. Castellanos-Gomez, Chem. Soc. Rev. **44**, 3691 (2015).
[8] B. Huang, G. Clark, D. R. Klein, D. MacNeill, E. Navarro-Moratalla, K. L. Seyler, N. Wilson, M. A. McGuire, D. H. Cobden, D. Xiao *et al.*, Nat. Nanotechnol. **13**, 544 (2018).
[9] C. Gong, L. Li, Z. Li, H. Ji, A. Stern, Y. Xia, T. Cao, W. Bao, C. Wang, Y. Wang *et al.*, Nature (London) **546**, 265 (2017).
[10] N. Sivadas, S. Okamoto, X. Xu, C. J. Fennie, and D. Xiao, Nano Lett. **18**, 7658 (2018).
[11] T. Song, Z. Fei, M. Yankowitz, Z. Lin, Q. Jiang, K. Hwangbo, Q. Zhang, B. Sun, T. Taniguchi, K. Watanabe *et al.*, Nat. Mater. **18**, 1298 (2019).
[12] P. Jiang, C. Wang, D. Chen, Z. Zhong, Z. Yuan, Z.-Y. Lu, and W. Ji, Phys. Rev. B **99**, 144401 (2019).
[13] W. Chen, Z. Sun, Z. Wang, L. Gu, X. Xu, S. Wu, and C. Gao, Science **366**, 983 (2019).
[14] Y. Deng, Y. Yu, Y. Song, J. Zhang, N. Z. Wang, Z. Sun, Y. Yi, Y. Z. Wu, S. Wu, J. Zhu *et al.*, Nature (London) **563**, 94 (2018).
[15] J. Li, Y. Li, S. Du, Z. Wang, B.-L. Gu, S.-C. Zhang, K. He, W.-H. Duan, and Y. Xu, Sci. Adv. **5**, eaaw5685 (2019).
[16] M. M. Otrokov, I. P. Rusinov, M. Blanco-Rey, M. Hoffmann, A. Yu. Vyazovskaya, S. V. Eremeev, A. Ernst, P. M. Echenique, A. Arnau, and E. V. Chulkov, Phys. Rev. Lett. **122**, 107202 (2019).
[17] J. Li, C. Wang, Z. Zhang, B. L. Gu, W. H. Duan, and Y. Xu, Phys. Rev. B **100**, 121103(R) (2019).
[18] D. Zhang, M. Shi, T. Zhu, D. Xing, H.-J. Zhang, and J. Wang, Phys. Rev. Lett. **122**, 206401 (2019).
[19] Y. Gong, J. Guo, J. Li, K. Zhu, M. Liao, X. Liu, Q. Zhang, L. Gu, L. Tang, X. Feng *et al.*, Chin. Phys. Lett. **36**, 089901 (2019).
[20] C. Liu, Y. Wang, H. Li, Y. Wu, Y. Li, J. Li, K. He, Y. Xu, J. Zhang, and Y. Wang, Nat. Mater. **19**, 522 (2020).
[21] Y. Deng, Y. Yu, M. Z. Shi, Z. Guo, Z. Xu, J. Wang, X. H. Chen, and Y. Zhang, Science **367**, 895 (2020).
[22] R. C. Vidal, H. Bentmann, T. R. F. Peixoto, A. Zeugner, S. Moser, C.-H. Min, S. Schatz, K. Kißner, M. Unzelmann, C. I. Fornari *et al.*, Phys. Rev. B **100**, 121104(R) (2019).
[23] A. Zeugner, F. Nietschke, A. U. B. Wolter, S. Gaß, R. C. Vidal, T. R. F. Peixoto, D. Pohl, C. Damm, A. Lubk, R. Hentrich *et al.*, Chem. Mater. **31**, 2795 (2019).
[24] Y.-J. Hao, P. Liu, Y. Feng, X.-M. Ma, E. F. Schwier, M. Arita, S. Kumar, C. Hu, R. Lu, M. Zeng *et al.*, Phys. Rev. X **9**, 041038 (2019).
[25] J. Ge, Y. Liu, J. Li, H. Li, T. Luo, Y. Wu, Y. Xu, and J. Wang, Nat. Sci. Rev. nwaa089 (2020).
[26] H. X. Fu, C. X. Liu, and B. H. Yan, Sci. Adv. **6**, eaaz0948 (2020).
[27] M. Z. Hasan and C. L. Kane, Rev. Mod. Phys. **82**, 3045 (2010).
[28] X.-L. Qi and S.-C. Zhang, Rev. Mod. Phys. **83**, 1057 (2011).
[29] X.-L. Qi, T. L. Hughes, and S.-C. Zhang, Phys. Rev. B **78**, 195424 (2008).
[30] J. E. Moore, Nature (London) **464**, 194 (2010).
[31] R. S. K. Mong, A. M. Essin, and J. E. Moore, Phys. Rev. B **81**, 245209 (2010).
[32] See Supplemental Material at http://link.aps.org/supplemental/10.1103/PhysRevB.102.081107 for discussions on methods, theoretical analysis of interlayer magnetic coupling, and guiding principles to tune interlayer magnetism, which includes Refs. [10–13,15,17,33–40].
[33] G. Kresse and J. Furthmüller, Phys. Rev. B **54**, 11169 (1996).
[34] J. P. Perdew, K. Burke, and M. Ernzerhof, Phys. Rev. Lett. **77**, 3865 (1996).
[35] K.-W. Lee and W. E. Pickett, Phys. Rev. B **83**, 180406 (2011).
[36] A. D. Becke and E. R. Johnson, J. Chem. Phys. **124**, 221101 (2006).
[37] S. Grimme, J. Antony, S. Ehrlich, and H. Krieg, J. Chem. Phys. **132**, 154104 (2010).
[38] Q. Wu, S. Zhang, H.-F. Song, M. Troyer, and A. A. Soluyanov, Comput. Phys. Commun. **224**, 405 (2018).
[39] J. B. Goodenough, *Magnetism and the Chemical Bond*, Vol. 1 (Wiley-Interscience, New York, 1963).
[40] E. Koch, Exchange mechanisms, in *Correlated Electrons: From Models to Materials*, edited by E. Pavarini, E. Koch, F. Anders, and M. Jarrell, Lecture Notes of the Autumn School Correlated Electrons 2012 Vol. 2 (Forschungszentrum Jülich, Jülich, 2012).
[41] J. Li, J. Y. Ni, X. Y. Li, H.-J. Koo, M.-H. Whangbo, J. S. Feng, and H. J. Xiang, Phys. Rev. B **101**, 201408 (2020).
[42] Y. H. Matsuda, Z. W. Ouyang, and H. Nojiri, Phys. Rev. Lett. **103**, 046402 (2019).
[43] J. Emsley, *The Elements*, 3rd ed. (Clarendon, Oxford, U.K., 1998).
[44] K. Li and D. Xue, J. Chem. Phys. A **110**, 11332 (2006).

[45] X. Wan, A. M. Turner, and A. Vishwanath, Phys. Rev. B **83**, 205101 (2011).
[46] F. D. M. Haldane, Phys. Rev. Lett. **61**, 2015 (1988).
[47] R. Yu, W. Zhang, H. Zhang, S.-C. Zhang, X. Dai, and Z. Fang, Science **329**, 61 (2010).
[48] A. A. Burkov and L. Balents, Phys. Rev. Lett. **107**, 127205 (2011).
[49] G. Xu, H. Wen, Z. Wang, X. Dai, and Z. Fang, Phys. Rev. Lett. **107**, 186806 (2011).
[50] B. Q. Lv, H. M. Weng, B. B. Fu, X. P. Wang, H. Miao, J. Ma, P. Richard, X. C. Huang, L. X. Zhao, G. F. Chen *et al.*, Phys. Rev. X **5**, 031013 (2015).
[51] B. Q. Lv, N. Xu, H. M. Weng, J. Z. Ma, P. Richard, X. C. Huang, L. X. Zhao, G. F. Chen, C. E. Matt, F. Bisti *et al.*, Nat. Phys. **11**, 724 (2015).
[52] S.-Y. Xu, I. Belopolski, N. Alidoust, M. Neupane, G. Bian, C. Zhang, R. Sankar, G. Chang, Z. Yuan, and C.-C. Lee, Science **349**, 613 (2015).
[53] C.-C. Lee, S.-Y. Xu, S.-M. Huang, D. S. Sanchez, I. Belopolski, G. Chang, G. Bian, N. Alidoust, H. Zheng, M. Neupane *et al.*, Phys. Rev. B **92**, 235104 (2015).
[54] B. H. Yan and C. Felser, Annu. Rev. Condens. Matter Phys. **8**, 337 (2017).
[55] A. A. Soluyanov, D. Gresch, Z. Wang, Q. S. Wu, M. Troyer, X. Dai, and B. A. Bernevig, Nature (London) **527**, 495 (2015).
[56] C.-Z. Chang, J. Zhang, X. Feng, J. Shen, Z. Zhang, M. Guo, K. Li, Y. Ou, P. Wei, L.-L. Wang *et al.*, Science **340**, 167 (2013).
[57] C.-Z. Chang, W. Zhao, D. Y. Kim, H. Zhang, B. A. Assaf, D. Heiman, S.-C. Zhang, C. Liu, M. H. W. Chan, and J. S. Moodera, Nat. Mater. **14**, 473 (2015).
[58] A. M. Turner, Y. Zhang, R. S. K. Mong, and A. Vishwanath, Phys. Rev. B **85**, 165120 (2012).
[59] R.-X. Zhang, F. C. Wu, and S. D. Sarma, Phys. Rev. Lett. **124**, 136407 (2020).
[60] J. W. Xiao and B. H. Yan, 2D Mater. **7**, 045010 (2020).